



Project 019 Development of Aviation Air Quality Tools for Airshed-Specific Impact Assessment: Air Quality Modeling

University of North Carolina at Chapel Hill

Project Lead Investigator

Saravanan Arunachalam, Ph.D.
Research Professor
Institute for the Environment
University of North Carolina at Chapel Hill
100 Europa Drive, Suite 490
Chapel Hill, NC 27517
919-966-2126
sarav@email.unc.edu

University Participants

University of North Carolina at Chapel Hill (UNC)

- PI: Saravanan Arunachalam, Research Professor and Deputy Director
- FAA Award Number: 13-C-AJFE-UNC Amendments 1-12
- Period of Performance: September 10, 2019 to September 30, 2020
- Tasks: Development of a framework for a new dispersion model for aircraft sources.

Project Funding Level

FAA provided \$350,064 in funding. Matching cost-share was provided by the Los Angeles World Airports (LAWA) and Environmental Defense Fund (EDF).

Investigation Team

Prof. Saravanan Arunachalam (UNC) (Principal Investigator) [Tasks 1, 2, 3, 4]
Dr. Chowdhury Moniruzzaman (UNC) (Co-Investigator) [Task 4]
Dr. Gavendra Pandey (UNC) (Co-Investigator) [Task 4]
Prof. Akula Venkatram (University of California, Riverside) (Consultant) [Task 4]

Project Overview

Aviation is predicted to grow steadily in upcoming years;¹ thus, a variety of aviation environmental policies will be required to meet emission reduction goals in aviation-related air quality and health impacts. Tools are needed to rapidly assess the implications of alternative policies for an evolving population and atmosphere. In the context of the International Civil Aviation Organization (ICAO)'s Committee on Aviation Environmental Protection (CAEP), additional approaches are required to determine the implications of global aviation emissions.

The overall objective of this project is to develop a new aircraft-specific dispersion model and continue the development and implementation of tools, both domestically and internationally, to allow for an assessment of year-to-year changes in significant health outcomes. These tools must be acceptable to the FAA (in the context of Destination 2025) and/or other decision-makers. More importantly, this new model must have the capability to address the 1-hour form of the NO₂ National Ambient Air Quality Standard (NAAQS) in the U.S., as well as support National Environmental Policy Act (NEPA) and/or NAAQS analyses that may be needed by airports. The developed methods must also rapidly provide output in order to support a

¹ Boeing Commercial Airplane Market Analysis, 2010.

variety of “what if” analyses and other investigations. While the tools for use within and outside the U.S. need not be identical, a number of goals are desirable for both cases:

- Enable the assessment of premature mortality and morbidity risks due to aviation-attributable particulate matter (PM) having diameter up to 2.5- μm (PM_{2.5}), ozone, and other pollutants known to exert significant health impacts;
- Capture airport-specific health impacts at regional and local scales;
- Account for the impact of landing/takeoff (LTO) versus non-LTO emissions, including a separation of effects;
- Allow for an assessment of a wide range of aircraft emission scenarios, including differential growth rates and emission indices;
- Account for changes in non-aviation emissions;
- Allow for assessments of sensitivity to meteorology;
- Provide domestic and global results;
- Include quantified uncertainties and differences with respect to Environmental Protection Agency (EPA) practices, which are to be minimized when scientifically appropriate; and
- Be computationally efficient such that tools can be used in time-sensitive rapid turnaround contexts and for uncertainty quantification.

During this period of performance, The University of North Carolina at Chapel Hill's Institute for the Environment (UNC-IE) team was expected to perform research on multiple fronts, as described below. However, the FAA has requested that Tasks 1–3 be placed on hold because the collaborative ASCENT Project 18 at BU did not receive funding from the FAA during FY2019. Thus, our report is limited to our progress on Task 4.

1. Create Boston Logan International Airport emission inventories.
2. Create a WRF-SMOKE-CMAQ modeling application.
3. Perform a model–monitoring intercomparison at Boston Logan International Airport.
4. Develop a new dispersion model for aircraft sources.

Task 4 – Develop a Framework for a New Dispersion Model for Aircraft Sources

University of North Carolina at Chapel Hill

Objectives

The FAA’s Aviation Environmental Design Tool (AEDT) is currently coupled with the U.S. EPA’s AERMOD dispersion model for modeling aircraft sources and is the required regulatory model in the U.S. for modeling airport-level aircraft operations during landing and takeoff cycles.

Recent studies have shown several limitations in the use of AERMOD for modeling aircraft sources. The Airport Modeling Advisory Committee (AMAC) developed a series of recommendations in 2011 to improve modeling jet exhaust. Since then, Airport Cooperative Research Program (ACRP) project 02-08 developed a guidance for airport operators on conducting measurement and modeling for air quality at airports, published in ACRP Report 70 (Kim et al., 2012). This study conducted a measurement and modeling study at Washington Dulles International Airport (IAD). More recently, ACRP project 02-58 developed a final report ACRP Report 171 (Arunachalam et al., 2017a) for providing dispersion modeling guidance for airport operators for local air quality and health. This study applied four different dispersion models—AERMOD, CALPUFF, SCICHEM, and the U.K.’s ADMS-Airport—for the Los Angeles International Airport (LAX) and compared modeled predictions with high resolution measurements taken during the Los Angeles Air Quality Source Apportionment Study (AQSAS). All these reports identified several limitations with AERMOD and developed a series of recommendations for improving dispersion modeling of aircraft emissions for airport-level air quality.

UNC recently developed the C-AIRPORT dispersion model for application to LAX (Arunachalam et al., 2017c). Initially, C-AIRPORT was designed to be part of the C-TOOLS series of community-scale, web-based modeling systems. The objective of C-TOOLS was to create a web-based interface to model multiple source types for short-term or long-term pollutant concentration averages and perform various what-if scenarios that assess the changes in air quality at local scales due to changes in inputs. C-AIRPORT uses a line-source based approach to model aircraft sources, based upon the C-LINE modeling system (Barzyk et al., 2015), and preliminary evaluation of the algorithms against LAX AQSAS was conducted.



Under previous year's funding, UNC-IE developed a comprehensive plan or a modeling framework that addresses known limitations from the above Tasks and proposed a viable and most suitable approach for modeling pollutants from aircraft sources. The primary objective of this plan is to demonstrate that a robust, improved pollutant dispersion model for aircraft can be developed for U.S. regulatory compliance purposes. The proposed new model will disperse pollutants from aircraft sources in a more technically and scientifically advanced manner (when compared to current AERMOD capabilities), with the ultimate goal of becoming a potential U.S. regulatory compliance tool, based on ongoing discussions between FAA and EPA. This plan will include an itemized list of known limitations along with a corresponding proposed developmental approach with recommendations on how to address them.

As part of this Task, we proposed implementing the plan with specific focus on three broad areas, over a period of two years.

Our approach would be to ensure that the new model will be "robust" and based on the state-of-science on source and plume characterization and the associated algorithms.

a) Source Characterization

This area looks at alternate options beyond the current area source-based approach in the AERMOD model. Some approaches we explored include:

- Volume treatment in AERMOD.
- Puff-based treatment like in SCICHEM.
- Line-based treatment like in C-AIRPORT.
- Line-puff or Jet Sources like in ADMS-Airport.

b) Physical Processes

This area will look at all relevant processes for aircraft dispersion including treatment of plume rise, wing tip vortices, low wind speed conditions, etc. Some specific approaches include:

- Coupled plume rise—wake model for assessing the effects of wake vortices on plume rise, dispersion, and ground-level concentrations.
- An integral approach called the Fluid-mechanical Entrainment model (FEM), which has been evaluated against LIDAR observations from Heathrow Airport (see Arunachalam et al., 2017a).

c) Chemical Processes

This area will look at adequate treatment of chemical conversion relevant to LTO cycles, such as NO_x-to-NO₂ (see Kinney et al., 2016), PM_{2.5} (see Arunachalam et al., 2017a), etc. Some approaches include:

- AERMOD includes the Plume Volume Molar Ratio Method (PVMRM), the Ozone Limiting Method (OLM), and the Ambient Ratio Method (ARM). But these methods are designed primarily for emissions from tall stacks there is thus a need for algorithms specific to aircraft sources.
- OLM neglects photolysis of NO₂ during the daytime and is thus likely to overestimate NO₂ concentrations. Further, OLM does not account for gradual background O₃ entrainment into the plume and does not account for the NO/NO₂ ratio depending on engine power.
- Similarly, for PM_{2.5}, we consider bringing in background estimates to account for secondary PM_{2.5} or look at other reduced-form chemical schemes.
- In both cases, we will review newer approaches that decouples transport from the chemistry as described in Venkatram et al., 1998 and implemented in ADMS-Airport by Carruthers et al., and more recently in R-LINE as described in Valencia et al., 2017.

Research Approach

In this research, we describe progress made on four fronts.

1. Diagnostic Evaluation of Observations from LAX AQSAS

1.1 Brief Description of LAX AQSAS

LAX is situated within the South Coast Air Basin (Basin). LAX is close to residential neighborhoods to the north, south, and east. The impact of airport operations on air quality is a key public health concern for the population surrounding this or any airport. For illustration, the NO_x and SO_x concentration measurements from the Los Angeles Source Apportionment Study (LAX AQSAS III) conducted at LAX in 2012 have been utilized. The air quality monitoring during Phase III was done in two separate six-week field measurement campaigns: "winter monitoring season" from January 31, 2012 to March 13, 2012 and "summer monitoring season" from July 18, 2012 to August 28, 2012. Three types of monitoring sites (four "core," four

“satellite,” and nine “gradient”), with different combinations of continuous monitors and time-integrated (24-hour and 7-day) samples, were used to determine how the ambient concentrations of various chemical species of interest vary by location, time of day, day of the week, and season (Figure 1.1). There are two main airfield runways at LAX, namely the South Airfield and the North Airfield. The most extensive air quality measurements were obtained at the four core sites. These core sites were identified in the study as the “Community East (CE)” site, the “Community North (CN)” site, the “Community South (CS)” site, and the “Air Quality (AQ)” site. The core monitoring station CE was in Lennox approximately one mile east of the South Airfield Runways and approximately one-third mile east of the I-405 Freeway. The CN core monitoring station was in Westchester approximately one mile east of the North Airfield Runways. The CS core monitoring station was located at the former Imperial Avenue School in El Segundo, approximately 600 feet from the LAX southern boundary. The fourth core monitoring station, AQ, was located at the South Coast Air Quality Management District (SCAQMD) Hastings site, which was northwest of the airport in Playa del Rey (Figure 1.1) (Arunachalam et al., 2017, ACRP Report 179). In this study, we have used only the NO_x and SO_x concentration measurements from these four core sites, collected in February 2012.



Figure 1.1. Location of core, gradient and satellite monitoring stations during LAX AQSAS Phase III (Arunachalam et al., 2017, ACRP Report 179).

During February 2012, morning winds were from the northeast until about 11:00 AM, resulting in greater contributions from non-airport emissions at the CE and CN sites, whereas in daytime and nighttime, the LAX airport was consistently downwind as winds were westerly during this time (Figure 1.2).

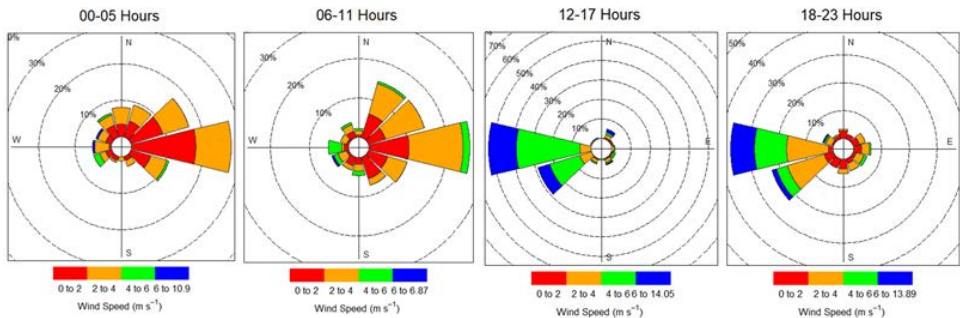


Figure 1.2. Wind rose plots for LAX during February 2012.

To understand the plume behavior at the LAX airport, we did an extensive observation analysis with the main species such as NO_x and SO_x. The hourly observed NO_x concentrations are plotted on each day of February 2012 in the form of line plots at all four core sites (AQ, CN, CS, and CE) (Figure 1.3). The peak in NO_x concentrations at the sites CE and CN, during the weekdays (Monday through Friday) can be attributed due to morning commute period (on-road vehicle emissions, mainly local traffic in the region north of the I-405 and east of the I-405 freeways (Figure 1.1) (Figure 1.3)). On the other hand, the significantly lower concentrations during the same time period on Sundays (February 5, 12, 19, and 26, 2012) provide additional confirmation of this source contribution. It appears that CN and CE sites were potentially impacted by airport NO_x emissions from the late morning to evening during February 2012. The CE and CN sites were downwind of LAX during consistent westerly winds from about 11:00 AM to 10:00 PM. LAX was downwind of all the core sites during this time of the day except the CS site. The CS site was impacted during a relatively brief period from about 06:00 AM to 11:00 AM, whereas the morning data from the AQ site show little evidence of impact from airport NO_x emissions (Figure 1.3). However, sources southeast of the study area include refineries and seaports, potentially impacted the observed concentrations at all four core sites, especially the CS and CN sites (Figure 1.1).

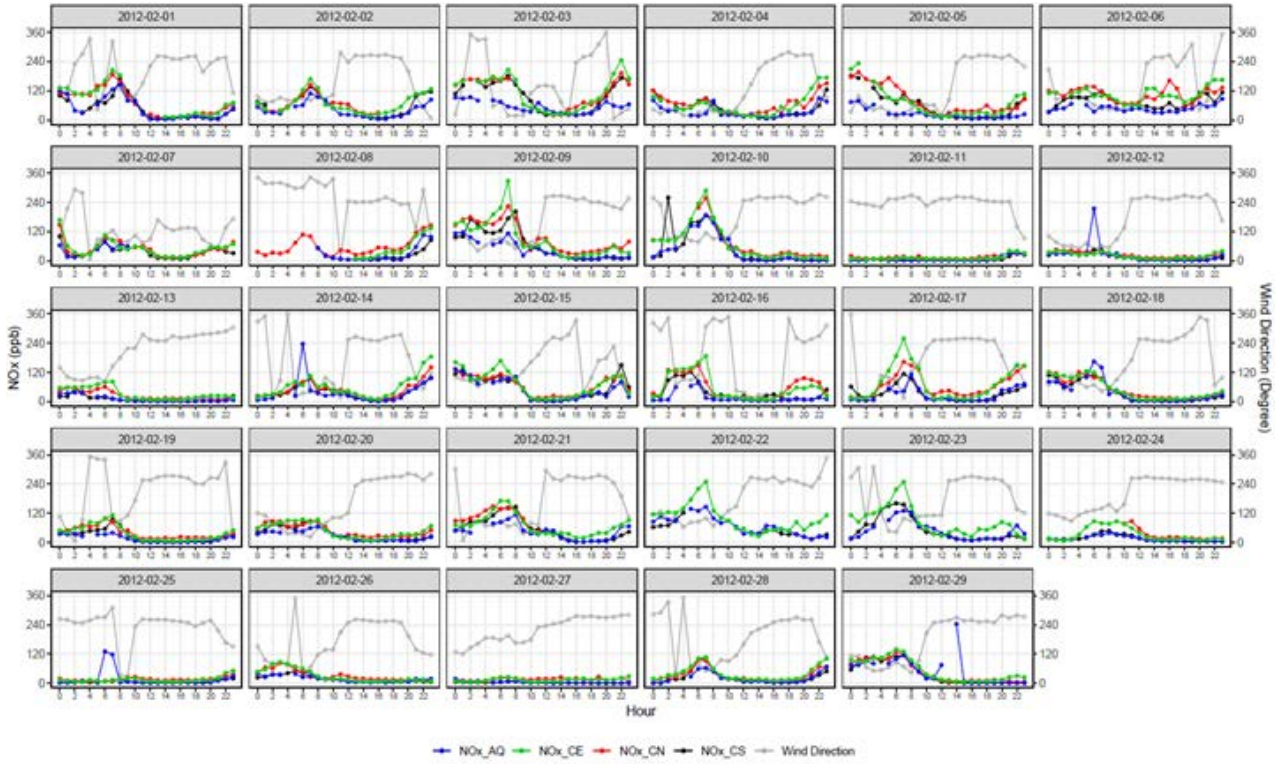


Figure 1.3. Daily Observed NO_x concentrations and wind direction at all four core (AQ, CN, CS, and CE) sites during February 2012 at LAX.

In contrast to NO_x, the SO_x concentrations were low during the morning period at all sites except the CS site. SO_x concentrations gradually increased throughout the day at both the CE and CN sites during February 2012. The relatively high SO_x concentrations were occurring at the CN site especially because this site was next to the North Airfield, as well as downwind during most of the time of the day in February 2012. The highest SO_x occurred on February 6 and 24, 2012 at the CN site (Figure 1.4). These results, coupled with the main source of SO_x, indicate airport emissions were the main source of SO_x at the CE and CN sites during February 2012.

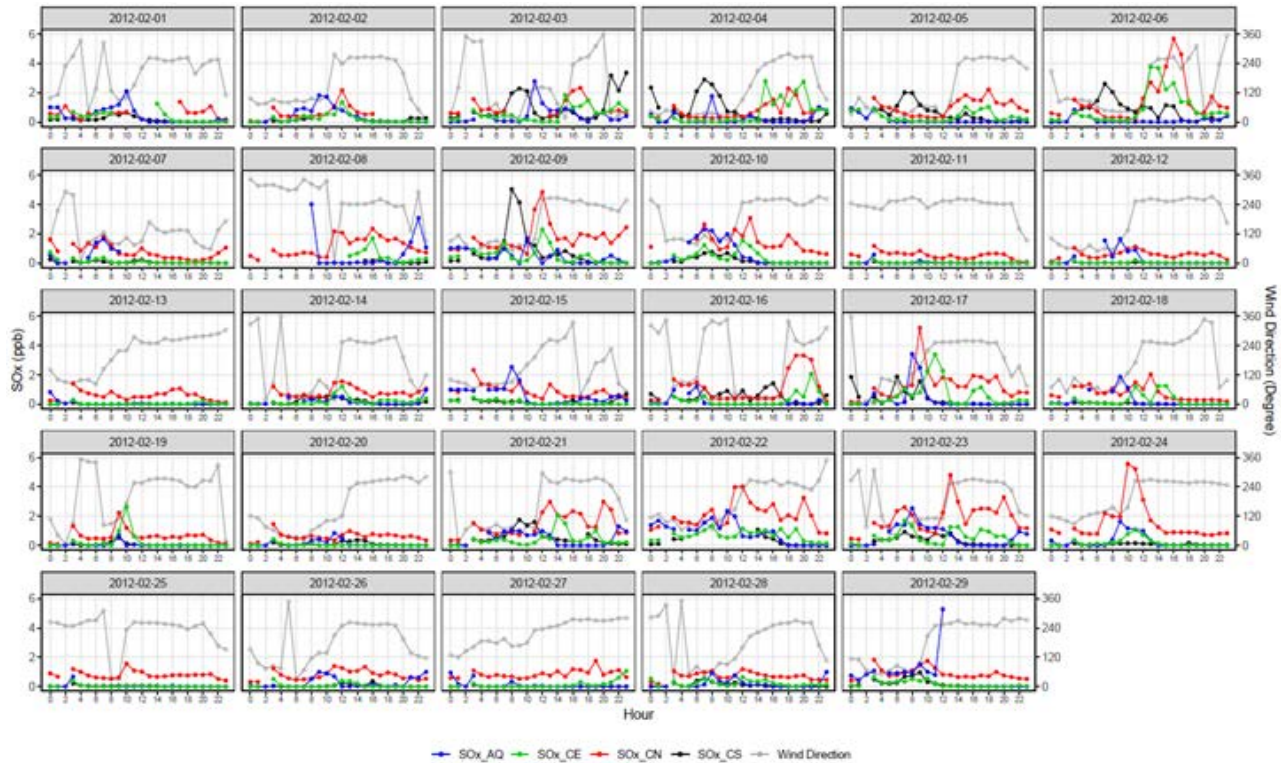


Figure 1.4. Daily observed SO_x concentrations and wind direction at all four core (AQ, CN, CS, and CE) sites during February 2012 at LAX.

1.2 Plume behavior at Core Sites

Bivariate polar plots are useful in understanding the plume behavior for different pollutants (here NO_x and SO_x) and a potential signal from aircraft operations (Carslaw et al., 2006). From Figure 1.5a and b displaying all four core sites (AQ, CN, CS, and CE), we can see that the observed NO_x and SO_x concentrations vary with both the wind speed and wind direction. In Figure 1.5a, the highest observed NO_x concentrations occur when the wind is blowing from the northeast at all four core sites. The highest NO_x concentrations vary little with wind speed. On the other hand, at the AQ site, the highest SO_x concentrations occur when the wind is blowing from the north with a speed of around 4 m/s (Figure 1.5b). At the CN site, the highest mean observed SO_x concentrations occur when the wind is coming from the southwest direction and at high wind speed around 4–5 m/s (Figure 1.5b). The unusual behavior of concentrations is due to the aircraft related operations as the CN site, which is located downwind of LAX most of the time during the day and it is next to the North Airfield (Figure 1.1). The CS site is located south of the South Airfield and it is largely impacted by the winds passing over the tall buildings of Los Angeles city (Figure 1.1). The peak observed SO_x concentration is from the northeast direction at high wind speed (Figure 1.5b). The site CE is largely impacted by its location next to major highways and it has less SO_x concentrations but large NO_x concentrations.

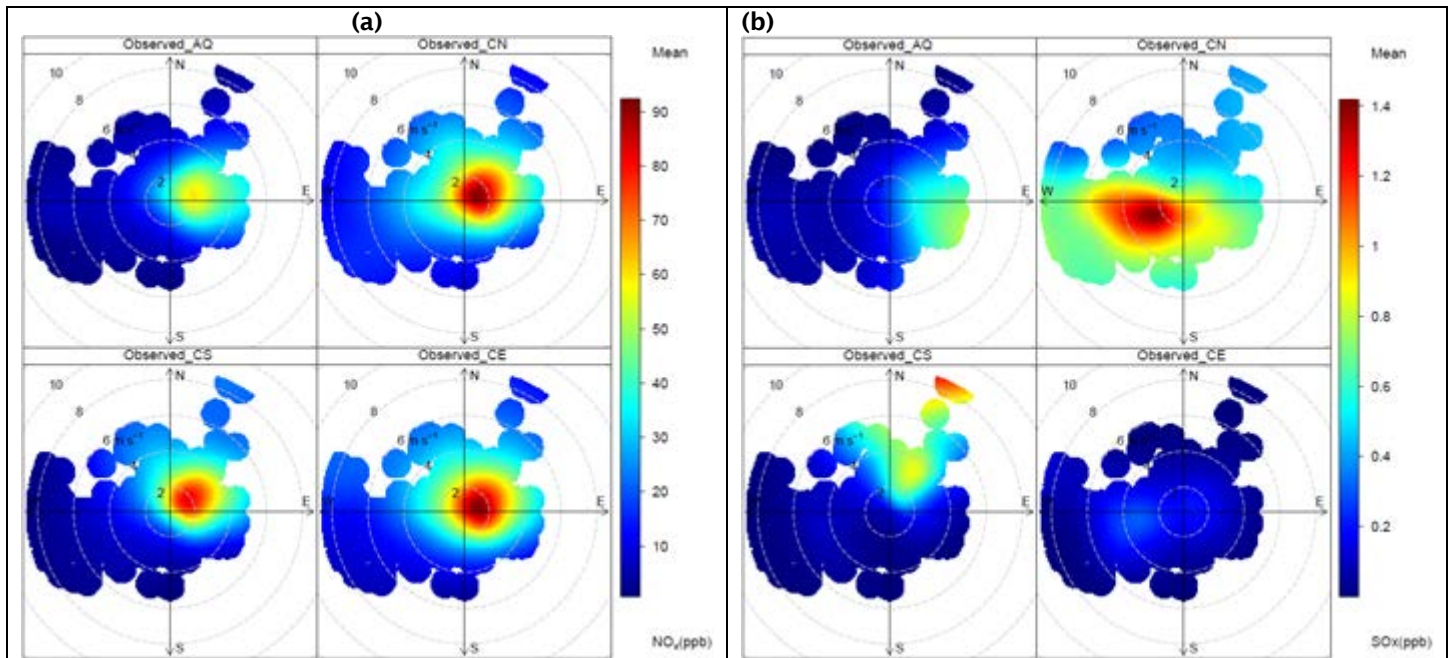


Figure 1.5. Bivariate polar plots of observed NO_x and SO_x concentrations at all four core (AQ, CN, CS, and CE) sites during February 2012 at LAX.

2. Emissions Processing of AEDT Emissions

AEDT-produced aircraft segmented data (termed hereafter as “AEDT-S” data) for both flight activity and emissions, provided by FAA to UNC-IE for LAX for February 2012, was used for the new Airport Dispersion Model (ADM) currently being developed at UNC-IE. The ADM needs the emission data of aircraft sources in the hourly emission rate in units of g/s for all the sources on the surface and in air. A Python-based emission processor code has been developed at UNC-IE which can postprocess the AEDT segment’s raw aircraft data to produce AMD-compatible hourly flight activity and emission rate data for any type of source characterization (area, line, volume, and point source). The AEDT-S data were compared with other emission processor data such as AEDT-area (AEDT-A) and EDMS-area (EDMS-A) (Arunachalam et al., 2017) for the AERMOD model.

2.1 Emissions Processing of AEDT-S Emissions

The AEDT-S file has time series flight segment data (each flight has about 45 segments), which has flight information including 3D location coordinates, aircraft and engine data, fuel burn, and emission data for 15 species. To produce the emission data in a desired format for the ADM, a Python-based emission processor has been developed at UNC-IE that can process the raw, high-temporal-resolution time series flight segment data and can produce the hourly emission rate (in g/s) and hourly flight activity (number of flights in an hour) for any desired source characterization.

2.1.1. Source characterization

The surface sources for the ADM model have been characterized as line-thermal source (which is an area source) aligned with the 19 rectangles shown in Figure 2.1. Out of these 19 rectangles, four rectangles (red color in Figure 2.1) are for four runways, further divided into four more sources (two directions and two LTOs) for each runway rectangle, making a total number of 31 surface sources (15 non-runway sources and 4x4 = 16 runway sources), listed and described in Table A1 in Appendix A1.

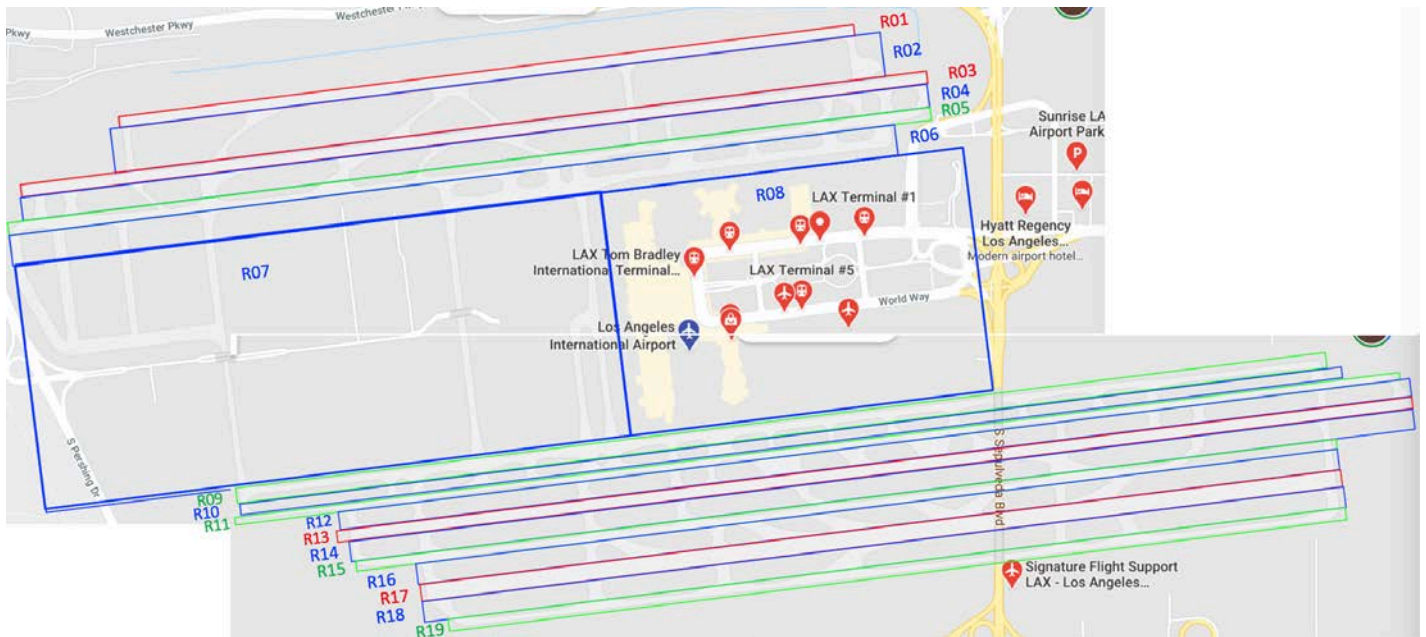


Figure 2.1. Airport runways, taxiways, terminal, and other areas have been divided into 19 horizontal rectangles (West to East) to extract emission data on surface sources. Four rectangles are for four runways (red rectangles), five rectangles are for the East-West taxiway (green rectangles), and 10 rectangles are for other areas such as ramps, taxiways, buildings, and grass (blue rectangles).

The source characterization in the ADM model (right column in Figure 2.2) is different than that of EDMS (left column in Figure 2.2) and AEDT (middle column in Figure 2.2) for the AERMOD model. The number of surface sources in ADM is lower than EDMS (Arunachalam et al., 2017) and AEDT, shown in Figure 2.2. The flight paths are not straight lines in the AEDT area and AEDT segment, unlike the EDMS area model shown in Figure 2.2. The hourly emission rate in the 31 surface area sources (listed in Table A1 in Appendix A) for 19 surface rectangles (shown in Figure 2.1) and in 144 air sources for nine air layers for each of the 16 flight paths (four runways x two directions x two LTOs) listed in Table A1 in Appendix A are determined using the AEDT segment's raw data.

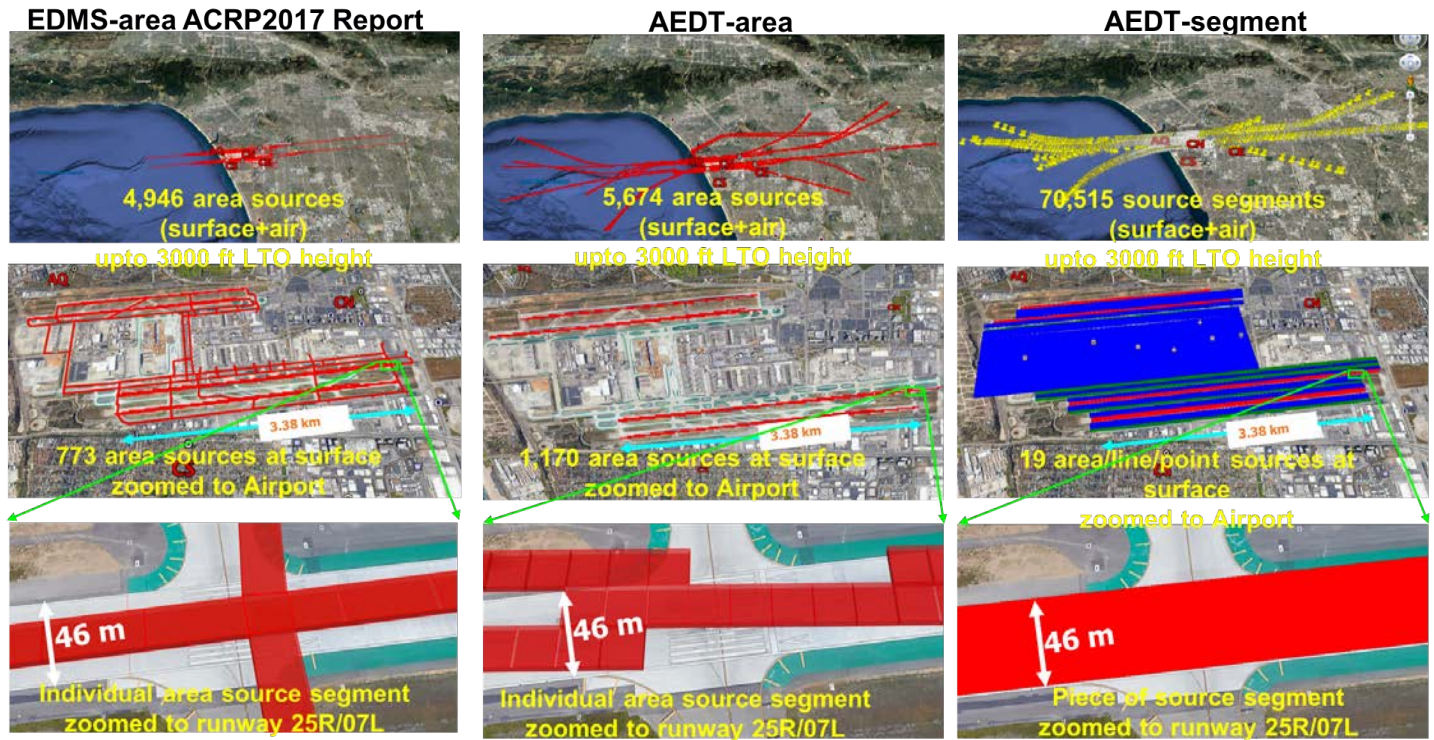


Figure 2.2. The source characterization in three emission processor models for aircraft sources. From left: EDMS-A, AEDT-A, and AEDT-S.

2.1.2. Preparation of Emissions Inputs for ADM

The AEDT segment flight and emission data were processed in three steps. In the first step, we extracted the data (making a smaller data set) by different categories. Then in the second step, the hourly flight number and emission rate for each of the sources are determined. In the third step, the non-aircraft source data (such as ground support equipment (GSE) and others) are determined by a correlation using a reference data (Arunachalam et al., 2013). The three steps are further described below.

Step 1:

1. Extract the data by a date.
2. Extract the data by the LTO cutoff height (3000 ft or 914 m).
3. Extract the data by eight AEDT LTO modes: 1) Taxi-out, 2) Takeoff ground, 3) Takeoff airborne, 4) Terminal climb, 5) Approach, 6) Landing ground roll, 7) Landing ground rolls with reverse thrust and 8) Taxi. The relative magnitudes of these eight LTO modes as a % of total emissions are shown in Figure A1 in Appendix A.
4. Extract surface data (having altitude up to 0 m) in 16 flight paths (four runways x two directions, two LTOs) for four runways and 15 non-runway rectangles using the user input latitude-longitude coordinates for each corner of the 19 rectangles shown in Fig. 2.1 and listed in Table A1 in Appendix A.
5. Extract air data for 144 air sources for nine air layers for each of the 16 flight paths (four runways x two directions x two LTOs) listed in Table A1 in Appendix A. The percentage of these nine air layers of the total emissions from LTO to 914 m are shown in Figure A2 in Appendix A. The latitude-longitude locations of the 144 air sources are shown in a Google Earth map in Figure A3 in Appendix A.

Step 2:

1. All the segmented emission data (emission amounts during a flight segment) are accumulated for each hour and then the hourly accumulated emissions are divided by 3,600 to estimate the hourly emission rate (g/s) for the above categories in Step 1. The number of flights are accumulated for each hour to get the hourly number of flights (#/hour) for the above categories in Step 1.



Step 3:

1. The AEDT segment data file does not have non-aircraft surface source emission data (such as GSE and others). The non-aircraft surface emission data are determined by a correlation using the AEDT-S’s total aircraft emission data and the ratio of non-aircraft source categories to the total aircraft source from a reference report (Arunachalam et al., 2013). These emissions are then distributed among the 15 non-runway surface rectangles by an approximation.

2.1.3. Source Characterization by LTO Mode.

Table 1 below lists the actual source type for each mode during LTO activity at LAX.

Table 1. Source characterization of eight AEDT LTO modes in the ADM

No	LTO modes	Source characterization
1	Taxi Out	Area
2	Takeoff Ground Roll	Area, line thermal
3	Takeoff Airborne	Point
4	Terminal Climb	Point
5	Approach	Point
6	Landing Ground Roll	Area, line thermal
7	Landing Ground Roll with Reverse Thrust	Area, line thermal
8	Taxi In	Area

2.2 Comparison of EDMS-A, AEDT-S, AEDT-A

The post-processed emission and flight data have been evaluated by comparing the data with other reference data.

2.2.1 Evaluation of flight activity data

The hourly flight activity data from AEDT-S were compared with the Los Angeles World Airport’s (LAWA’s) actual flight data (LAWA, 2020) for February 6, 2012, shown in Figure 2.3 and Table A2 in Appendix A. The flight activity in AEDT-S for LAX’s four runways have similar hourly flight activity to LAWA’s actual data and the differences between the AEDT-S model and the LAWA actual data were from 1 to 6%, shown in Table A2 in Appendix A.

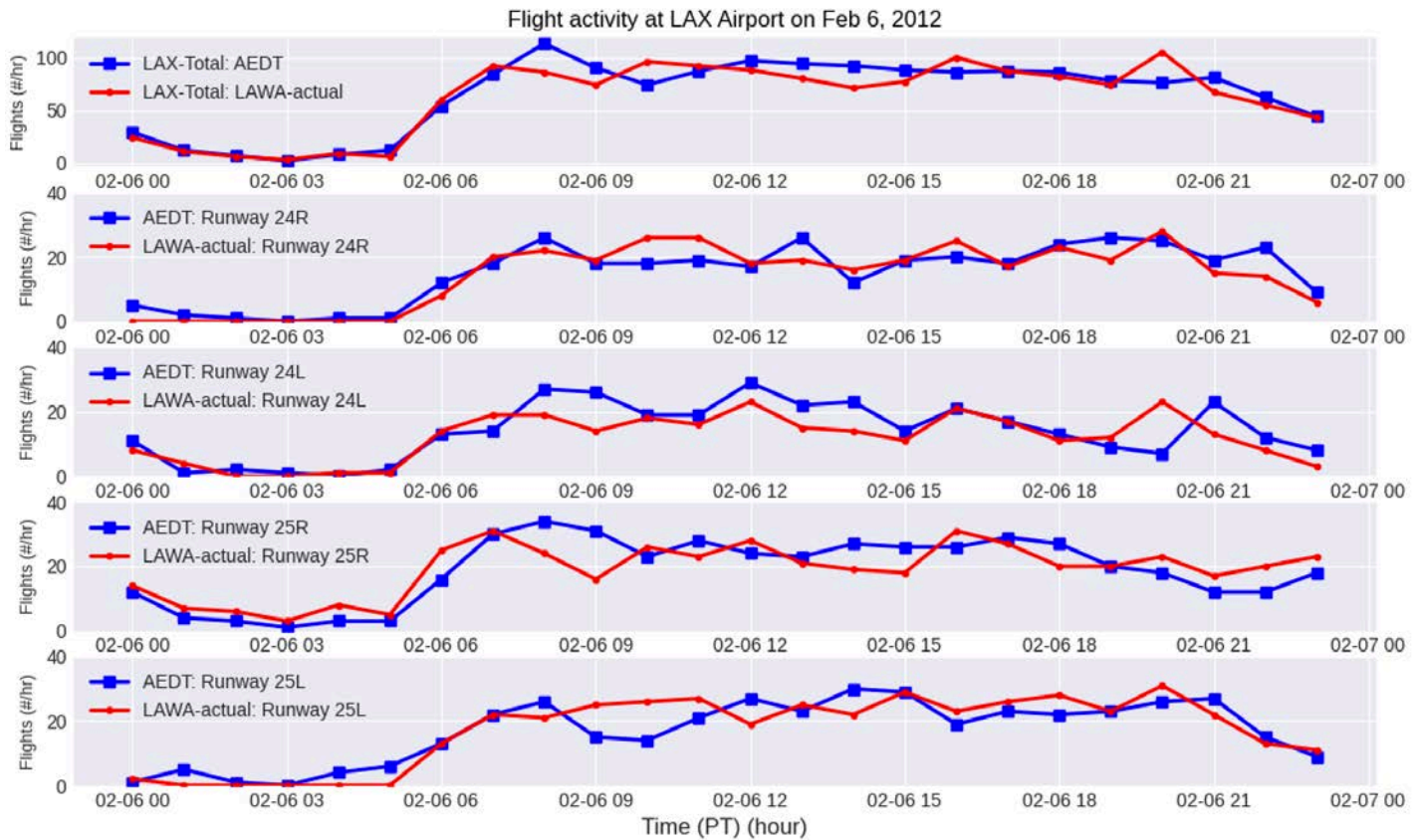


Figure 2.3. Hourly flight activity at LAX on February 6, 2012 by AEDT and LAWA-actual for total LTO.

2.2.2 Evaluation of emission data of AEDT-S comparing with AEDT-A and EDMS-A data

The hourly NO_x and SO_x emission rate by AEDT-S emission processor was compared with the AEDT-A and EDMS-A (Arunachalam et al., 2017) emission processor models for Feb 6, 2012 at LAX, shown in Figure 2.4. The emission rate of both NO_x (shown in Figure 2.4a, b, c) and SO_x by AEDT-S and AEDT-A were exactly matched, indicating that the AEDT-S emission processor's emission data are reasonable. The emission trends in AEDT-S and AEDT-A were consistent with the diurnal trend of EDMS-A both for NO_x (shown in Figure 2.4a, b, c) and SO_x (shown in Figure 2.4 d, e, f). The EDMS-A NO_x and SO_x emissions were overpredicted at the surface (shown in Figure 2.4a and d, respectively) and underpredicted in air (shown in Figure 2.4b and e, respectively) when compared with AEDT-S and AEDT-A, likely due to differences in the altitude cutoff used in EDMS versus AEDT for the different configurations.

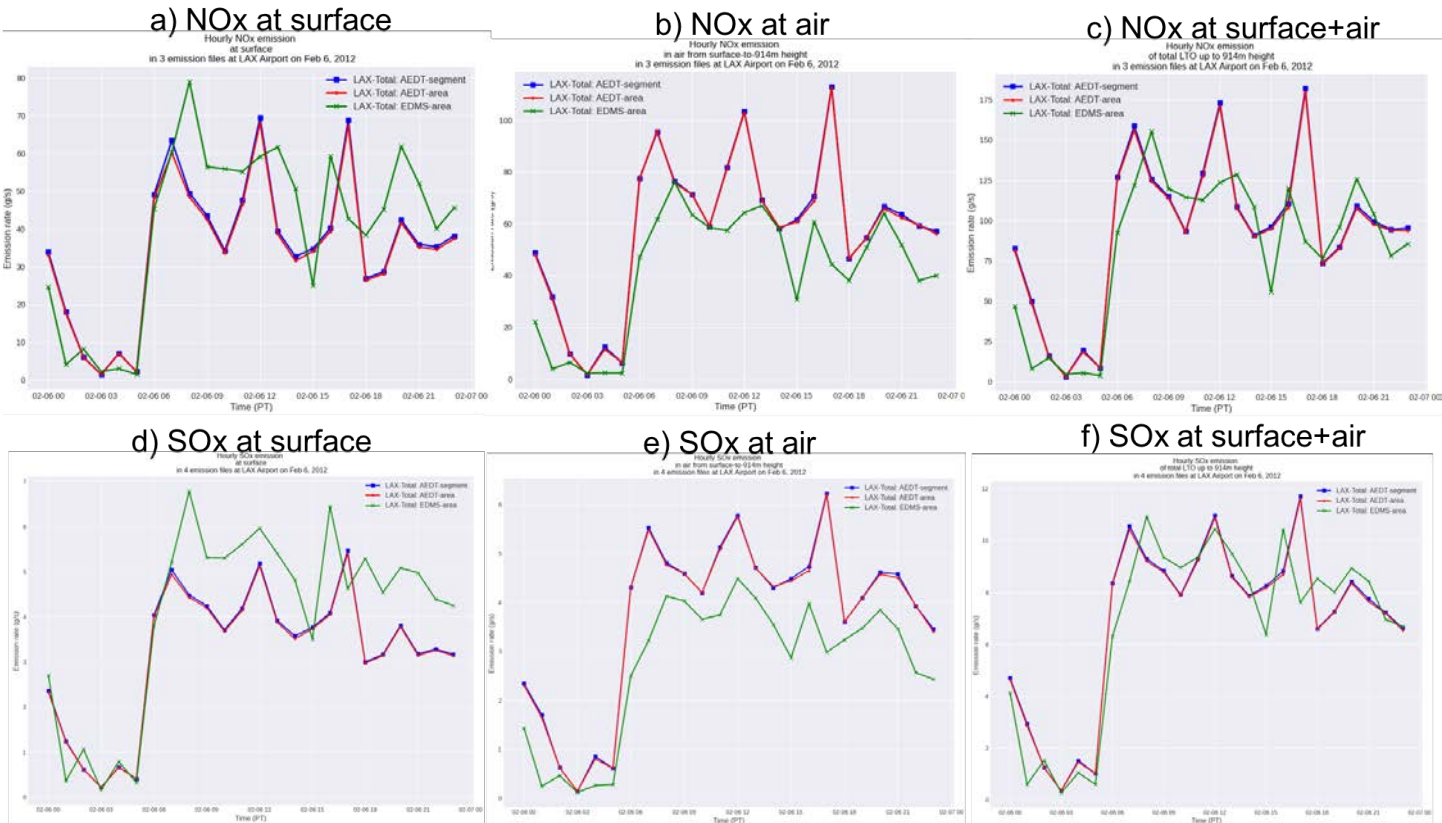


Figure 2.4. Hourly NOx and SOx emission rate at LAX on Feb 6, 2012 by AEDT-S (blue line), AEDT-A (red line), and EDMS-A (green line) for NOx (top row) a) LTO-surface, b) LTO-air from surface to 914 m (3000 ft) and c) LTO total-surface-&-air 914m and for SOx (bottom row) d) LTO-surface, e) LTO-air from surface to 914 m (3000 ft) and f) LTO total-surface-&-air 914m.

3. Alternate Treatment of Meteorological Inputs

3.1 Methodology

When an airport is situated near a shoreline, where meteorological conditions significantly vary from spatial uniformity, an added complexity occurs during dispersion. In this condition, the airport region neither becomes unstable nor very stable due to the cold breeze from the ocean. The input preprocessor (AERMET) of AERMOD does not account for important features of the boundary layer that occurs on the shoreline, where many of the large U.S. airports are situated. In this study, we have modified the meteorological outputs from AERMET as discussed below to account for formation of the internal boundary layer, where stable air from the ocean flows onto the warmer land surface of the airport. Based on this, we have done a sensitivity analysis for the meteorological input parameters of the AERMOD and evaluated the AERMOD model by comparing model estimates of SOx with measurements made during February 2012 from the Los Angeles Source Apportionment Study (LAX AQSAS III) conducted at LAX. The measurements consisted of 1-hour averaged concentrations made at the four core sites, AQ, CN, CS, and CE, shown in Figure 1.1. For this analysis, we have taken the emissions from the EDMS emission inventory of LAX accounting for all the airport sources. The sensitivity analysis led to the following changes:

- To account for the shoreline effect at LAX, stable and convective conditions in the AERMET file are replaced by neutral conditions: the Monin-Obukhov length is set to 1000 m, and the friction velocity is computed using the neutral formulation,

$$u_* = kU_r / \ln(z_r / z_0)$$

where k is the von-Karman constant, U_r is the wind speed at Z_r (reference height), and Z_0 is the roughness length.



- Roughness lengths (Z_0) altered when the winds blew from the northeast quadrant, reflecting the flow passing over the tall buildings in Los Angeles' urban core.

3.2 Simulated Results

The performance of the AERMOD model is assessed at all the four core sites using 1) diurnal variation of concentrations averaged over the month, and 2) quantile-quantile (Q-Q) plots constructed with 1-hour averaged concentrations measured during the 29 days of February. In addition, model performance is also characterized using fractional bias (FB) of the robust highest concentrations (RHC) using the procedures described in Cox and Tikvart (1990). The U.S. EPA recommends this metric to measure performance of models that are used in regulatory applications. A negative/positive value of FB indicates an over/under prediction of the observed concentrations. We have calculated the factor of two (FAC2) to the observations..

3.2.1 Diurnal variation of concentrations averaged over the month

The diurnal variation of concentrations averaged over the month at all four core sites (AQ, CN, CS, and CE) are exhibited in the form of diurnal line plots for both observed and AERMOD model predicted concentrations with interquartile range for original as well as modified meteorology (Figures 3.1 and 3.2).

At the AQ site, there are two observed peaks above 2 ppb, in the early morning and afternoon, that the model underestimates for both meteorological conditions (Figures 3.1 and 3.2). The model predictions have a large peak in late evening for both meteorological conditions. However, with the modified meteorology, the model predicted lowering concentrations in comparison to the original meteorology. There is little correspondence between the observed and modeled diurnal patterns for both meteorological conditions (Figures 3.1 and 3.2).

The modeled concentrations above 0.8 ppb are higher than the measured values at the CN site, and the model shows a large peak in the late evening with the original meteorology. After modifying the model inputs based on the neutral and roughness change, the model predictions are improved and closer to the observed diurnal behavior from 10 AM onward, whereas in the early morning, the model is still underestimating the observed diurnal concentrations. On the other hand, the correlation coefficient is improved from -0.30 to 0.38 (Figures 3.1 and 3.2).

The CS site is largely impacted by the emissions when the wind direction is from the northeast. We examined the possibility that the effective roughness seen by this site is governed by the flow over Los Angeles, where tall buildings can increase roughness. Therefore, we set the roughness length to 1.2 m when the wind is blowing from the northeast (Figure 1.2). The observed diurnal concentration has a single peak in morning, whereas the model has two large peaks (one in the morning and second in the late evening) with original meteorology (Figure 3.1). After applying the stability and roughness changes, the model predicted concentrations are closer to the observed diurnal concentrations, with the model able to slightly capture the morning observed peak, whereas the late evening peak is still missing. In addition, the correlation coefficient improves from 0.5 to 0.6 (Figures 3.1 and 3.2). We can say that the model predictions are getting close to observations after modifications in the meteorology at the CS site.

The model predictions are close to observations in the early morning to noon for both the original and modified meteorology. In the late evening, the model prediction has a large peak when run with original meteorology versus the modified meteorology (Figures 3.1 and 3.2). However, the model predictions are improved after modifications in meteorology.

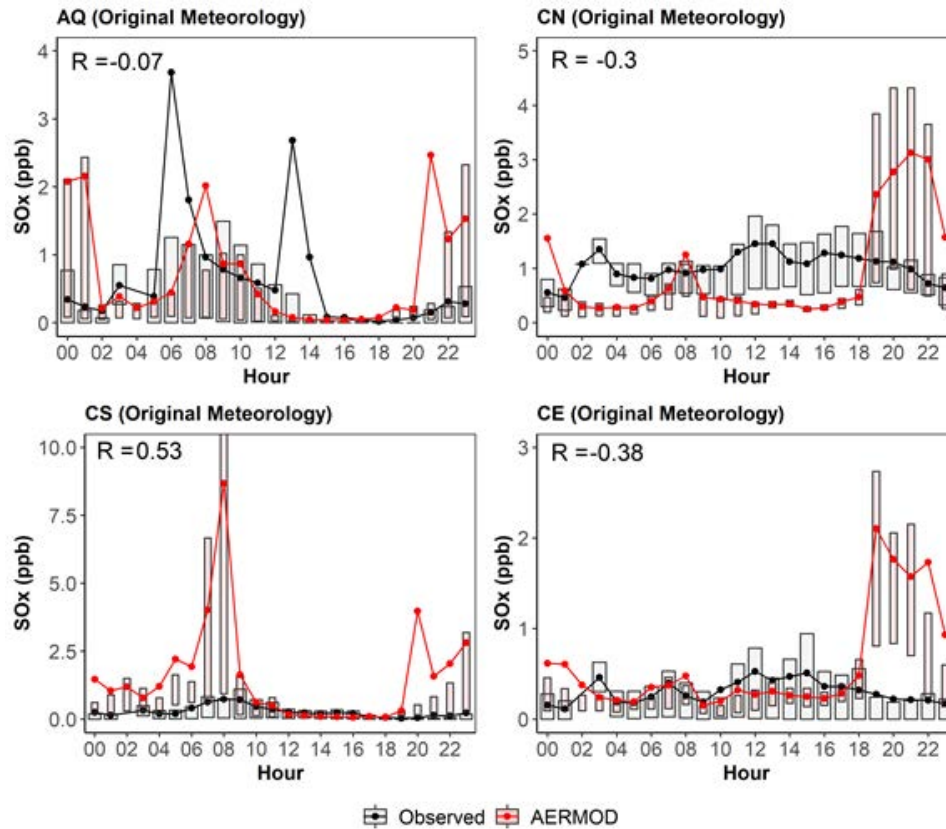


Figure 3.1. Diurnal variability in observed and modeled SOx concentrations with original meteorology at all four core sites (AQ, CN, CS, and CE). Bars represent interquartile ranges and lines represents mean of values.

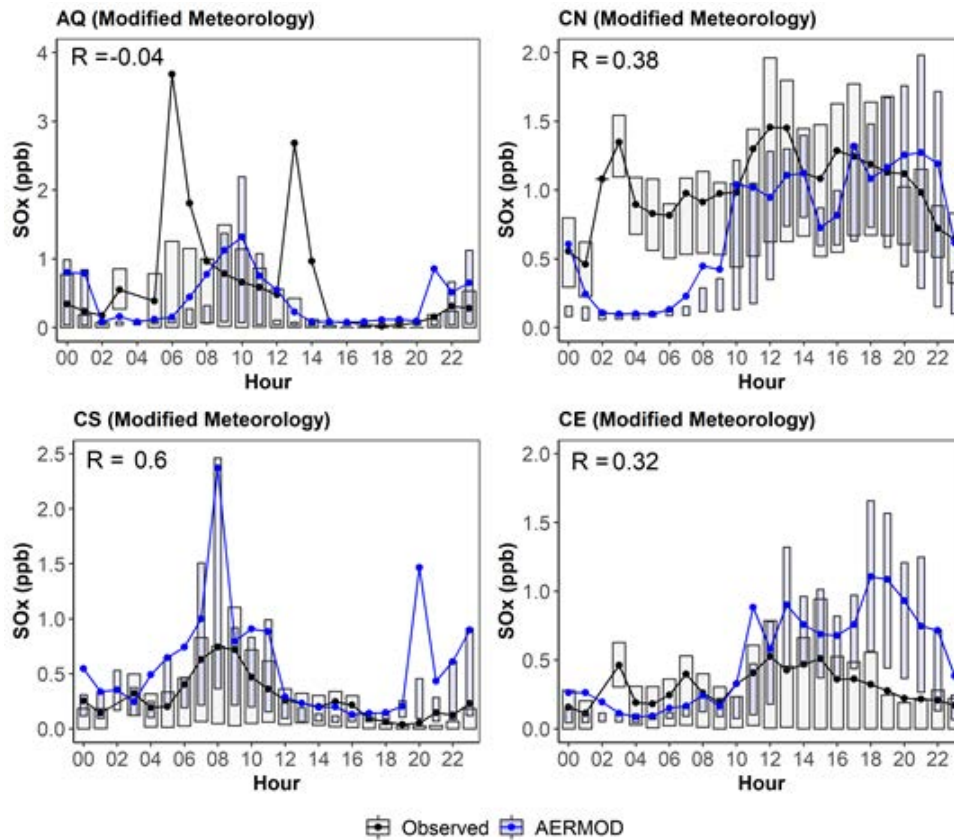


Figure 3.2. Diurnal variability in observed and modeled SO_x concentrations with modified meteorology at all four core sites (AQ, CN, CS, and CE). Bars represent interquartile ranges and lines represents mean of values.

3.2.2 Quantile-Quantile (Q-Q) distribution analysis

It is important to examine/evaluate the performance of a model for high concentrations because the assessment of the model for high ground-level concentrations, in compliance with air quality, is necessary (Weil et al., 1992). In unpaired concentration distribution plots or Q-Q plots, first the predictions and observations are ranked from highest to lowest and then both ranked predictions and ranked observations are plotted (Venkatram, 1999). The dotted (-----) line represents that the predicted concentrations are one-to-one to the observations. The solid lines of half and double slope indicate under and over-predictions, respectively.

At the AQ site, the highest concentrations are overpredicted by the model with original meteorology, whereas the concentrations from the middle to lower range are within the factor of two lines. On the other hand, with the modified meteorology, the lower concentrations are becoming less accurate, whereas the highest concentrations are getting closer to one-to-one line, which is very important for air quality assessment. However, the FAC2 is decreasing from 35% to 28% with modified meteorology (Figure 3.3).

For the CN site, the model is overpredicting the higher concentrations and underpredicts the middle to lower concentrations with original meteorology. On the other hand, with modified meteorology, the model is predicting the higher concentrations very close to the one-to-one line whereas it slightly underpredicts the lower concentrations (Figure 3.3). In addition, the FAC2 is improved from 33% to 50% after modification of the input parameters. The prediction of FAC2 greater than 50% is good for air quality assessment (Chang and Hanna, 2004). The fractional bias is also decreased from -0.99 to -0.21 (Figure 3.3).

At the CS site, the model is highly overpredicting the concentrations with original meteorology, this leads to the negative FB. After applying the modifications in the input parameters, we can easily see that the improvements from the figure 3.3. The

overall concentration is getting close to the one-to-one line with modified meteorology (Figure 3.3). The FB is decreased from -1.62 to -1.07 whereas the FAC2 to the observations is improved substantially from 0 to 27% (Figure 3.3).

The CE site shows little change after the modifications to the input parameters. The higher concentrations are getting closer to the one-to-one line with modified meteorology. The FB is improved from -1.13 to -0.52 and FAC2 is almost the same (Figure 3.3).

Hence, overall, the higher concentrations are getting close to the one-to-one line after modifications in the input meteorological parameters. From all the above analysis, we can say that the meteorology matters a lot, and suggests the need to re-examine the meteorology that governs concentrations at AQ. Note that we obtain the best results when it is assumed that stable conditions govern the concentrations at this site. However, apart from this aspect, there are additional issues related to source characterization and treatment of physical and chemical processes that will be addressed as part of the ADM development.

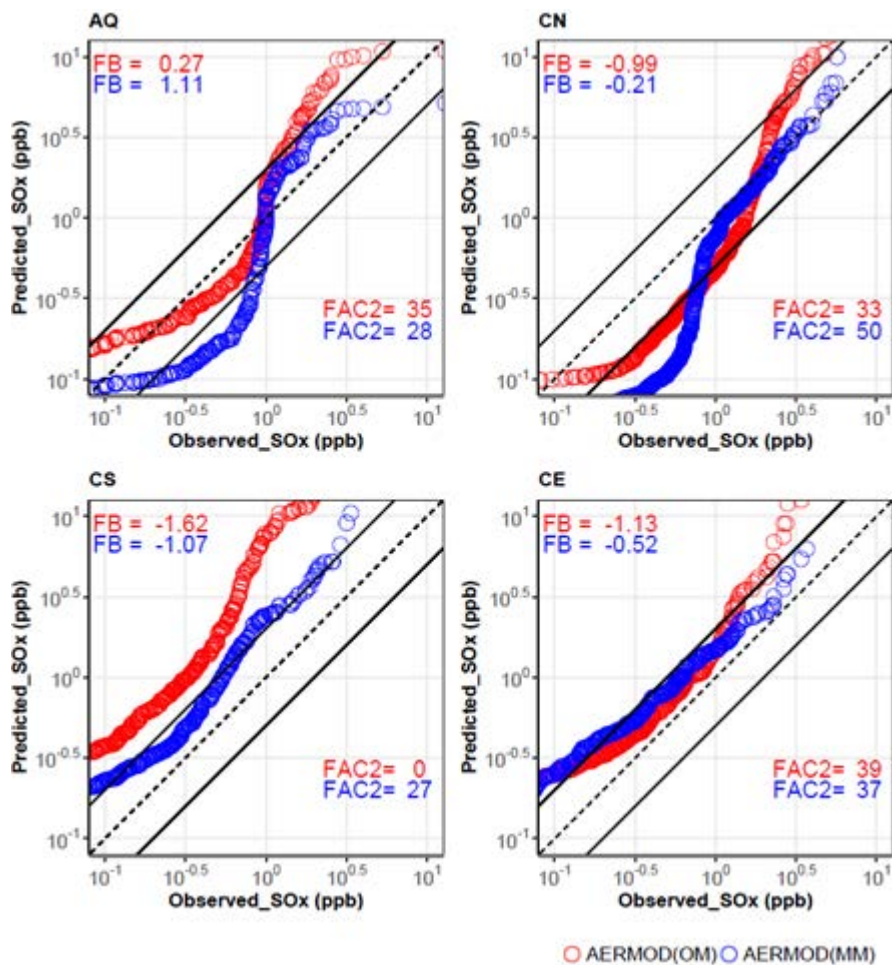


Figure 3.3. Quantile-quantile plots between observed and modeled SOx concentrations with original (red color) and modified meteorology (blue color) at all four core sites (AQ, CN, CS, and CE).



4. Development of Airport Dispersion Model (ADM)

4.1 Model Algorithm Development

We developed and tested code to treat dispersion of emissions from different types of sources at LAX. The sources include aircraft during takeoff roll, climb out, and taxiing. Emissions along the runway are modeled as line sources or area sources. Each runway is described with two lines along the length of the runway, spaced by the width of the runway. The line sources include meandering and plume rise of jet exhaust described using the line thermal model.

The runway can be treated as an area source with plume rise modeled with an initial plume spread. Emissions during taxiing are also treated using area sources. The treatment of area sources differs from that used in models such as AERMOD in that vertical dispersion is modeled using the solution of the mass conservation equation. As shown by Nieuwstadt and van Ulden (1978), this solution provides a more realistic description of observations than the commonly used Gaussian distribution. Emissions during climb out in the air are modeled using point sources along the path of the aircraft after takeoff. The path is specified as an inclined line starting at the end of the runway and ending at 914 m (3000 ft), which is considered to be the height at which an aircraft starts reducing power.

4.2 Evaluation against LAX AQSAS

The main objective of this task is to develop a new airport dispersion model (ADM), that can address past issues involving aircraft dispersion modeling such as source characterization, unconventional plume behavior of the aircraft sources, and treatment of low wind and meander, etc. A new ADM is being developed that will address these issues. In the new ADM, we have characterized the aircraft sources as area sources (that are aligned, in a line, to each runway), airborne sources as point sources, and other aircraft-related sources as area sources. In this section, we discuss preliminary results of this ADM.

The preliminary results of predicted NO_x and SO_x concentrations (obtained from LAWA AQSAS study for February 2012 only) are in the form of diurnal line plots and Q-Q distribution for both the original (OM) and modified meteorology (MM) at all four core sites (AQ, CN, CS, and CN). We have also characterized the source in two ways: not including the plume rise with line thermal source (ADM), and inclusion of a plume rise algorithm with the line thermal source (ADM_PR). To simulate both models, we have utilized the emissions from AEDT-segment (ASA) calculations which are discussed in section 2 of this report. Here, in this study, we have modeled the aircraft sources only. In addition, model performance is also characterized using Fractional Bias (FB) of the robust highest concentrations (RHC) using the procedures described in Cox and Tikvart (1990). The USEPA recommends these metrics to measure performance of models that are used in regulatory applications.

4.2.1 NO_x concentration analysis

4.2.1.1 Without plume rise algorithm (ADM)

The ADM predicted NO_x diurnal concentrations with OM are slightly able to capture the morning peaks of observed diurnal concentrations, whereas after 9 AM to late evening, ADM underpredicts the observed concentrations at the AQ and CS sites. On the other hand, during this period at the CN and CS sites, ADM highly underpredicts the observed concentrations with original meteorology (Figure 4.1a).

In the Q-Q plots between ADM predicted and observed overall NO_x concentrations, the ADM predicted concentrations are close to the one-to-one observed line, but ADM highly underpredicts the middle-to-lower range concentration at all four core sites. ADM predicts approximately 9%, 7%, 11%, and 1% concentrations within the FAC2 at the AQ, CN, CS, and CE sites, respectively, with original meteorology (Figure 4.1b).

With the modified meteorology, the ADM highly underpredicts the NO_x concentrations most of the time as the values of FB are positive (Figure 4.1d). In capturing the diurnal behavior at all four core sites, ADM captures the observed diurnal pattern from noon to after noon at the CN site especially well (Figure 4.1c). In addition, and only at the AQ site, the ADM predicts 9% concentrations within a FAC2 with modified meteorology (Figure 4.1d).

4.2.1.2 With plume rise algorithm (ADM_PR)

The ADM_PR-predicted NO_x diurnal concentration highly underpredict the observed concentrations, most of the time during February 2012, with both the original and modified meteorology (Figure 4.1a and c). However, with both meteorology conditions, ADM_PR is capturing the pattern of observed NO_x concentrations (Figure 4.1a and c). In addition, the FAC2 is 1% by ADM_PR at the CS site only with both meteorological conditions.



Hence, we have modeled only the NOx emissions related to aircraft sources. Still, we are not taking account of or modeling most of the NOx emissions of other airport sources as well as non-airport sources, which were contributing during that time and especially at the CE site. This site was highly impacted by the on-road sources because CE was located next to the major highways. We are assuming that after including the other on-airport and off-airport sources in plume rise model (ADM_PR), we will be able to capture the diurnal patterns as well as the high concentrations, which is very important for air quality assessment especially at the CN and CS sites.

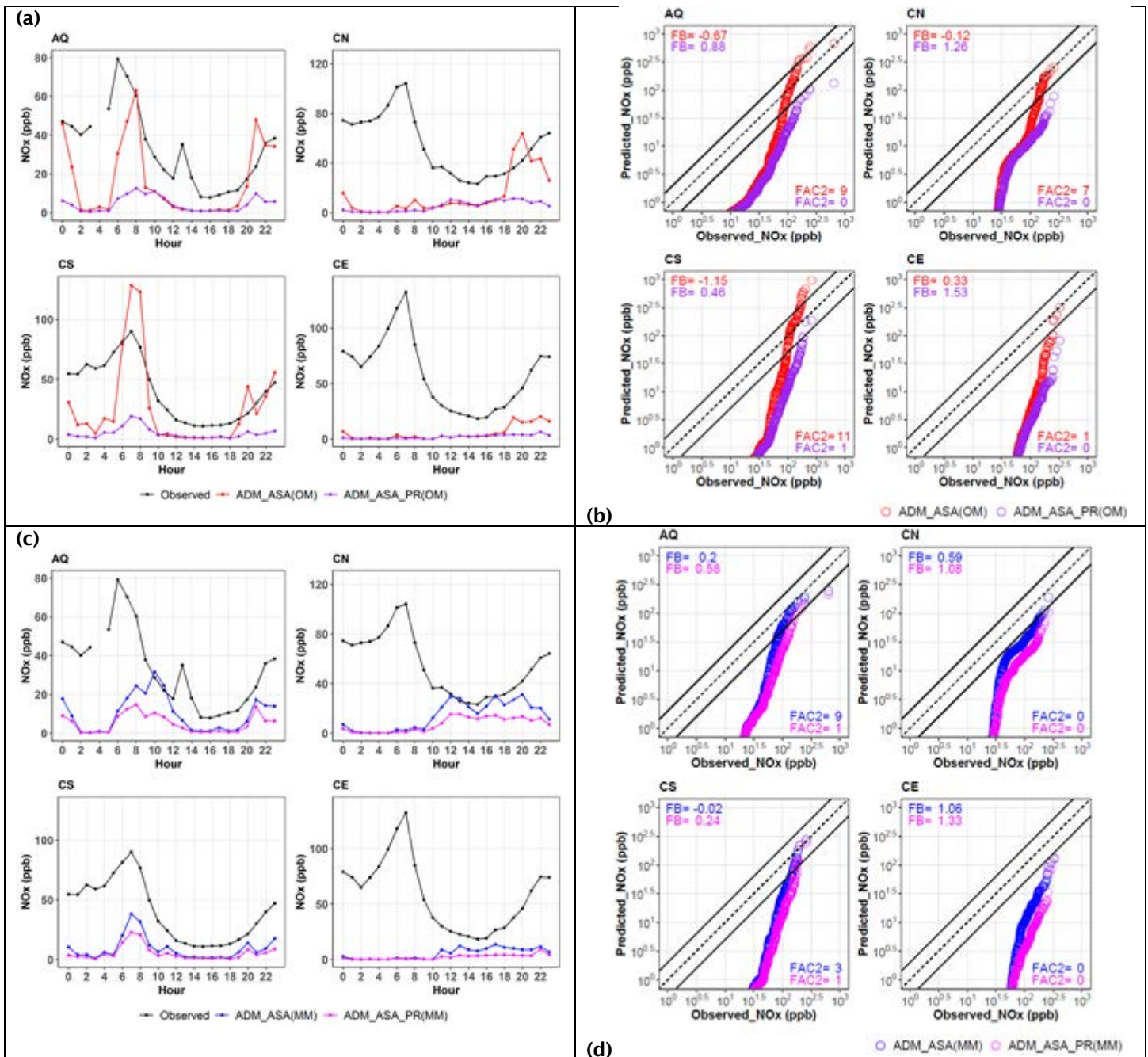


Figure 4.1. Diurnal variability (a and c) and Q-Q distribution (b and d) between observed (black) and modeled (ADM with and without plume rise) NOx concentrations with original (a and b) and modified meteorology (c and d) at all four core sites (AQ, CN, CS, and CE). The initialisms are as follows: ADM (Airport Dispersion Model); ASA (AEDT Segment Area); PR (With Plume Rise); OM (Original Meteorology); MM (Modified Meteorology).

4.2.2 SO_x concentration analysis

4.2.2.1 Without plume rise algorithm (ADM)

With original meteorology, the ADM-predicted SO_x diurnal concentrations are slightly able to capture the morning peak of diurnal observed concentrations at the AQ site whereas ADM is missing the second peak at the AQ. In addition, at all four core sites (AQ, CN, CS, and CE), the ADM is overpredicting the observed SO_x concentrations in late evening. During late morning to afternoon, ADM is underpredicting the observed concentrations at all four core sites with original meteorology. At the CS site, ADM substantially overpredicts the morning peak with original meteorology (Figure 4.2a).

However, with the modified meteorology, the diurnal patterns of the observed concentrations distribution are captured well by ADM, especially at the CN site, from late morning to the evening. In contrast, ADM is substantially underpredicting the observed concentration between 0:00 hours to 10:00 hours at all core sites, except CS. At the CS site during this period, ADM highly overpredicts the morning observed peak, but the prediction is improved from original meteorology (Figure 4.2d).

In the Q-Q plots between ADM-predicted and observed overall SO_x concentrations, the high concentrations are overpredicted by the ADM at all four core sites, whereas lower concentrations are underpredicted at the CN, CS, and CE sites with original meteorology (Figure 4.2b). ADM is predicting approximately 33%, 16%, 19%, and 19% concentrations within the FAC2 at the AQ, CN, CS, and CE sites, respectively, with original meteorology (Figure 4.1b).

On the other hand, with modified meteorology, the ADM-predicted high concentrations are close to the one-to-one line or within a factor of two lines at all four core sites. However, the middle-to-lower concentrations are still underpredicted by the ADM at all four core sites (Figure 4.2d). In addition, the values of FB are improved from -0.67, -1.61, and -0.81 to 0.29, -0.73, and 0.11 at the sites CN, CS, and CE, respectively, with original and modified meteorology. The values of FAC2 are improved from 33%, 16%, 19%, and 19% when using original meteorology to 44%, 44%, 40%, and 38% with the modified meteorology at the sites AQ, CN, CS, and CE, respectively (Figures 4.2(b and d)).

4.2.2.2 With plume rise algorithm (ADM_{PR})

ADM_{PR} either underpredicts or is close to the diurnal observed concentrations most of the time at all four core sites, whereas at the CS site, ADM_{PR} predicted morning peak is very close to the observed peak as compare to ADM (without plume rise) with original meteorology (Figure 4.2a).

Therefore, with the modified meteorology, the ADM- and ADM_{PR}-predicted diurnal concentrations are similar at the AQ and CS sites. At the other two sites, CN and CE, the ADM_{PR}-predicted concentrations are close to the ADM for 0:00 hours to 10:00 hours, whereas after 10 AM, the ADM_{PR} is slightly more underpredictive compared to ADM with modified meteorology (Figure 4.2c). However, there is a high peak with ADM_{PR} with modified meteorology at 10 PM at the CE site (Figure 4.2c).

As shown in Figure 4.2b, the ADM_{PR}-predicted high concentrations are getting close to the one-to-one line at the AQ and CS sites, whereas at the other two sites, ADM_{PR} underpredicts more with the original meteorology. In addition, the FAC2 improves from 19% to 46% at the CS site with ADM_{PR} (Figure 4.2b and d) with original meteorology.

On the other hand, with modified meteorology, ADM_{PR} predicts the high concentrations closer to the one-to-one line of observation at the AQ and CS sites than ADM with modified meteorology. However, at the other two sites, ADM_{PR} with modified meteorology more significantly underpredicts the high concentrations, whereas the lower concentrations are similar to ADM with modified meteorology (Figure 4.2d).

Hence, here, we have modeled only the SO_x emissions related to aircraft sources. Still, we are not taking into account a substantial contribution of emissions coming from the south of the South Airfield, where a Chevron refinery is situated beyond CS, as well as some of the SO_x on-airport and off-airport emissions. We expect that after including the contribution of these sources with plume rise model (ADM_{PR}), we will be able to capture the diurnal patterns as well as the high and low concentrations adequately at all four core sites.

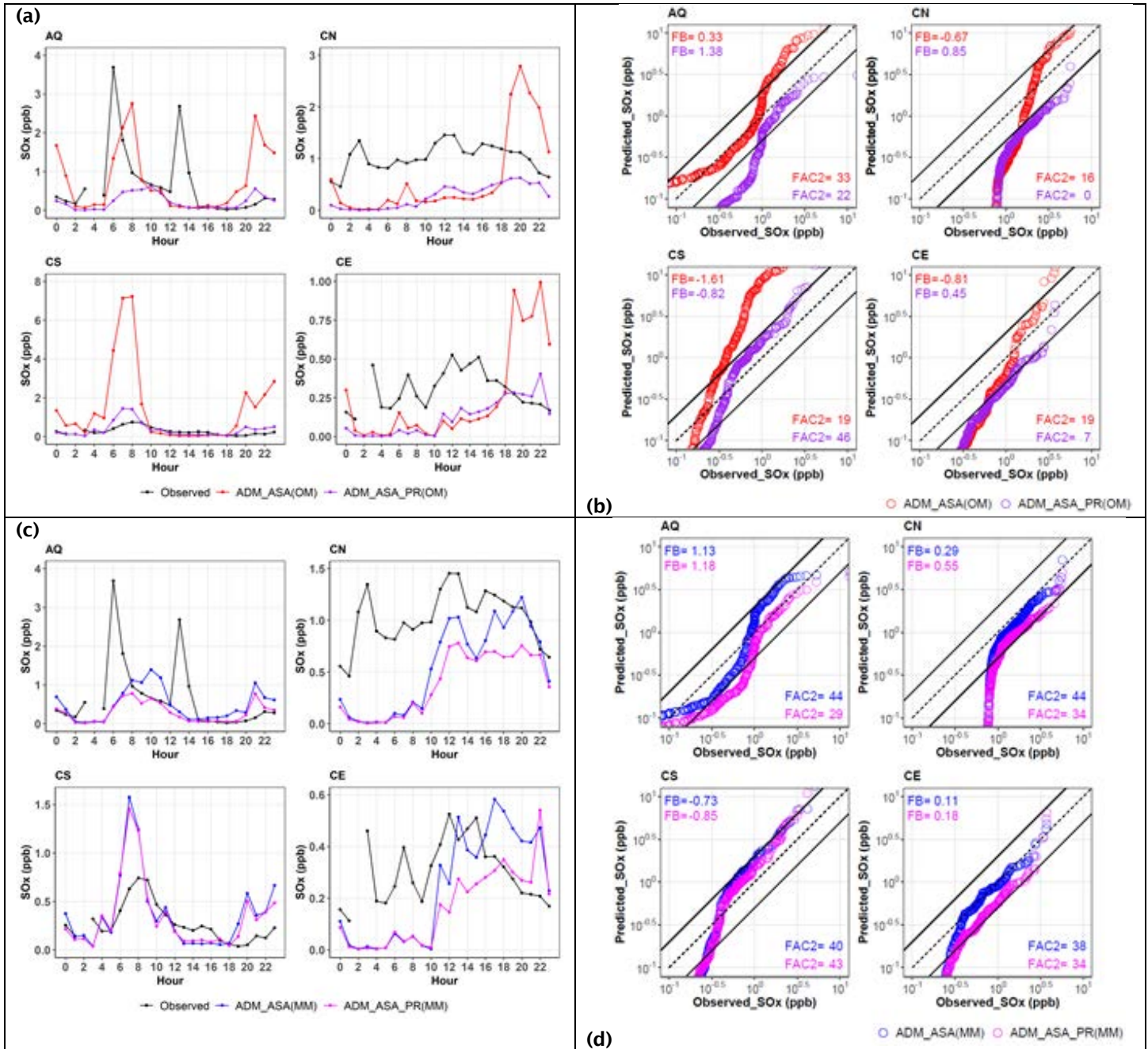


Figure 4.2. Diurnal variability (a and c) and Q-Q distribution (b and d) between observed and modeled (ADM with and without plume rise) SOx concentrations with original (a and b) and modified meteorology (c and d) at all four core sites (AQ, CN, CS, and CE). The initialisms are the same as those in Figure 4.1.

Milestone

We submitted a draft of the modeling results and code to the FAA. A revised version with additional cleanup and additional treatment of physical and chemical processes will be submitted.



Major Accomplishments

- Design document detailing features that will go into the new ADM.
- Initial conceptual approach for plume behavior at LAX using data from LAX AQSAS.
- Initial treatment of source characterization to treat aircraft sources during LTO cycles.
- Initial prototype of dispersion model to treat aircraft emissions at LAX and preliminary evaluation completed.

Publications

N/A

Outreach Efforts

Presentation at semi-annual ASCENT stakeholder meetings in the spring and fall of 2020, held virtually.
Presentation and collaborative discussion during monthly meetings with the FAA and EPA.

Awards

None

Student Involvement

None

Plans for Next Period

Finalize the ADM with all physical and chemical processes and complete evaluation.

References

- Arunachalam, S., Blanchard, C., Henry, R., Tombach, I., 2013. LAX Air Quality and Source Apportionment Study Volume 1. Executive Summary. Los Angeles World Airports [Available at: <https://www.lawa.org/lawa-environment/lax/lax-air-quality-and-source-apportionment-study/final-report-and-materials>]
- LAWA, 2020. LAWA Flight Data. Los Angeles World Airt. Flight Data, Obtained through Personal Communication.
- Arunachalam, S., A. Valencia, M. Woody, M. Snyder, J. Huang, J. Weil, P. Soucacos and S. Webb (2017). Dispersion Modeling Guidance for Airports Addressing Local Air Quality Concerns. Transportation Research Board Airport Cooperative Research Program (ACRP) Research Report 179, Washington, D.C. Available from: <http://nap.edu/24881>
- Arunachalam, S., Naess, B., Seppanen, C., Valencia, A., Brandmeyer, J.E., et al. (2019b). A new bottom-up emissions estimation approach for aircraft sources in support of air quality modelling for community-scale assessments around airports Akula Venkatram Jeffrey Weil Vlad Isakov and Timothy Barzyk. *Int. J. Environ. Pollut.* 65, 43-58. doi:10.1504/IJEP.2019.101832
- Carshaw, D. C., Beevers, S. D., Ropkins, K., Bell, M. C., 2006. Detecting and quantifying aircraft and other on-airport contributions to ambient nitrogen oxides in the vicinity of a large international airport. *Atmos. Environ.* 40, 5424-5434.
- Chang, J.C., Hanna, S.R., 2004. Air quality model performance. *Meteorol. Atmos. Phys.* 87, 167-196.
- Cox, W.M., Tikvart, J.A., 1990. A statistical procedure for determining the best performing air quality simulation model. *Atmos. Environ. Part A, Gen. Top.* 24, 2387-2395. [https://doi.org/10.1016/0960-1686\(90\)90331-G](https://doi.org/10.1016/0960-1686(90)90331-G)
- Nieuwstadt, F.T.M., van Ulden, A.P., 1978. A numerical study on the vertical dispersion of passive contaminants from a continuous source in the atmospheric surface layer. *Atmos. Environ.* 12, 2119-2124. [https://doi.org/10.1016/0004-6981\(78\)90166-X](https://doi.org/10.1016/0004-6981(78)90166-X)
- Valencia, A., S. Arunachalam, D. Heist, D. Carruthers, and A. Venkatram (2018). Development and Evaluation of the R-LINE Model Algorithms to Account for Chemical Transformation in the Near-road Environment, *Transp. Res. Part D: Transp. Environ.*, 59, 464 - 477.
- Venkatram, A., Du, S., Hariharan, R., Carter, W., Goldstein, R. (1998). The concept of species age in photochemical modeling. *Atmos. Environ.* 32. doi:10.1016/S1352-2310(98)00032-6
- Venkatram, A., 1999. Applying a framework for evaluating the performance of air quality models. In: Proceedings of the Sixth International Conference on Harmonisation within Atmospheric Dispersion Modeling for Regulatory Applications, Rouen, France, 11-14 October, 1999.
- Weil, J. C., Sykes, R. I., Venkatram, A., 1992. Evaluating air-quality models: review and outlook, *J. Applied Meteorol.* 31, 112-1145.



Appendix A: Emission processing

Table A1. The list and the description of the surface and air sources for the ADM model.

No	Source name	Description of sources
	Surface sources	
1	ER01R06L_TG	Surface emission (g/s) for Take-Off Ground (TG) West-to-East (06L) direction
2	ER01R24R_TG	Surface emission (g/s) for Take-Off Ground (TG) East-to-West (24R) direction
3	ER01R06L_LG	Surface emission (g/s) for Landing Ground (LG) West-to-East (06L) direction
4	ER01R24R_LG	Surface emission (g/s) for Landing Ground (LG) East-to-West (24R) direction
5	ER02	Surface emission (g/s) in rectangles "R02"
6	ER03R06R_TG	Surface emission (g/s) for Take-Off Ground (TG) West-to-East (06R) direction
7	ER03R24L_TG	Surface emission (g/s) for Take-Off Ground (TG) East-to-West (24L) direction
8	ER03R06R_LG	Surface emission (g/s) for Landing Ground (LG) West-to-East (06R) direction
9	ER03R24L_LG	Surface emission (g/s) for Landing Ground (LG) East-to-West (24L) direction
10	ER04	Surface emission (g/s) in rectangles "R04"
11	ER05	Surface emission (g/s) in rectangles "R05"
12	ER06	Surface emission (g/s) in rectangles "R06"
13	ER07	Surface emission (g/s) in rectangles "R07"
14	ER08	Surface emission (g/s) in rectangles "R08"
15	ER09	Surface emission (g/s) in rectangles "R09"
16	ER10	Surface emission (g/s) in rectangles "R10"
17	ER11	Surface emission (g/s) in rectangles "R11"
18	ER12	Surface emission (g/s) in rectangles "R12"
19	ER13R07L_TG	Surface emission (g/s) for Take-Off Ground (TG) West-to-East (07L) direction
20	ER13R25R_TG	Surface emission (g/s) for Take-Off Ground (TG) East-to-West (25R) direction
21	ER13R07L_LG	Surface emission (g/s) for Landing Ground (LG) West-to-East (07L) direction
22	ER13R25R_LG	Surface emission (g/s) for Landing Ground (LG) East-to-West (25R) direction
23	ER14	Surface emission (g/s) in rectangles "R14"
24	ER15	Surface emission (g/s) in rectangles "R15"
25	ER16	Surface emission (g/s) in rectangles "R16"
26	ER17R07R_TG	Surface emission (g/s) for Take-Off Ground (TG) West-to-East (07R) direction
27	ER17R25L_TG	Surface emission (g/s) for Take-Off Ground (TG) East-to-West (25L) direction
28	ER17R07R_LG	Surface emission (g/s) for Landing Ground (LG) West-to-East (07R) direction
29	ER17R25L_LG	Surface emission (g/s) for Landing Ground (LG) East-to-West (25L) direction
30	ER18	Surface emission (g/s) in rectangles "R18"
31	ER19	Surface emission (g/s) in rectangles "R19"



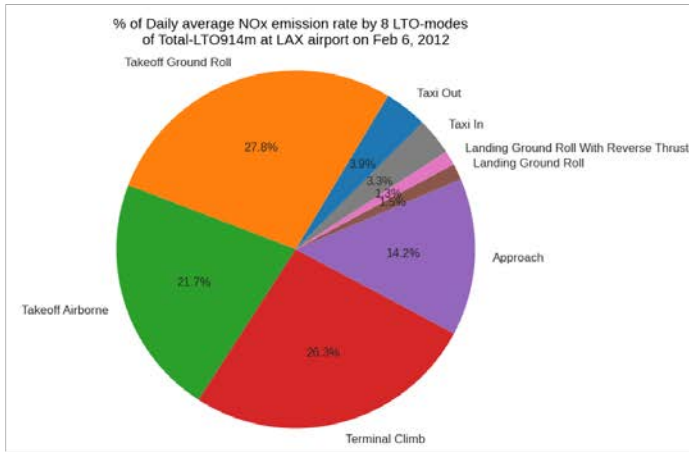
Air sources		
	Air-layer 01	Air-source for air-layer 01
32	ER01R06L_TA1	Air emission (g/s) for Take-Off (T) West-to-East (06L) direction in air layer 1 (altitudes 0 to 100 m)
33	ER01R24R_TA1	Air emission (g/s) for Take-Off (T) East-to-West (24R) direction in air layer 1 (altitudes 0 to 100 m)
34	ER01R06L_LA1	Air emission (g/s) for Landing (L) West-to-East (06L) direction in air layer 1 (altitudes 0 to 100 m)
35	ER01R24R_LA1	Air emission (g/s) for Landing (L) East-to-West (24R) direction in air layer 1 (altitudes 0 to 100 m)
36	ER03R06R_TA1	Air emission (g/s) for Take-Off (T) West-to-East (06R) direction in air layer 1 (altitudes 0 to 100 m)
37	ER03R24L_TA1	Air emission (g/s) for Take-Off (T) East-to-West (24L) direction in air layer 1 (altitudes 0 to 100 m)
38	ER03R06R_LA1	Air emission (g/s) for Landing (L) West-to-East (06R) direction in air layer 1 (altitudes 0 to 100 m)
39	ER03R24L_LA1	Air emission (g/s) for Landing (L) East-to-West (24L) direction in air layer 1 (altitudes 0 to 100 m)
40	ER13R07L_TA1	Air emission (g/s) for Take-Off (T) West-to-East (07L) direction in air layer 1 (altitudes 0 to 100 m)
41	ER13R25R_TA1	Air emission (g/s) for Take-Off (T) East-to-West (25R) direction in air layer 1 (altitudes 0 to 100 m)
42	ER13R07L_LA1	Air emission (g/s) for Landing (L) West-to-East (07L) direction in air layer 1 (altitudes 0 to 100 m)
43	ER13R25R_LA1	Air emission (g/s) for Landing (L) East-to-West (25R) direction in air layer 1 (altitudes 0 to 100 m)
44	ER17R07R_TA1	Air emission (g/s) for Take-Off (T) West-to-East (07R) direction in air layer 1 (altitudes 0 to 100 m)
45	ER17R25L_TA1	Air emission (g/s) for Take-Off (T) East-to-West (25L) direction in air layer 1 (altitudes 0 to 100 m)
46	ER17R07R_LA1	Air emission (g/s) for Landing (L) West-to-East (07R) direction in air layer 1 (altitudes 0 to 100 m)
47	ER17R25L_LA1	Air emission (g/s) for Landing (L) East-to-West (25L) direction in air layer 1 (altitudes 0 to 100 m)
	Air-layer 02	Air-source for air-layer 02 (from 100m to 200m)
...
...
...



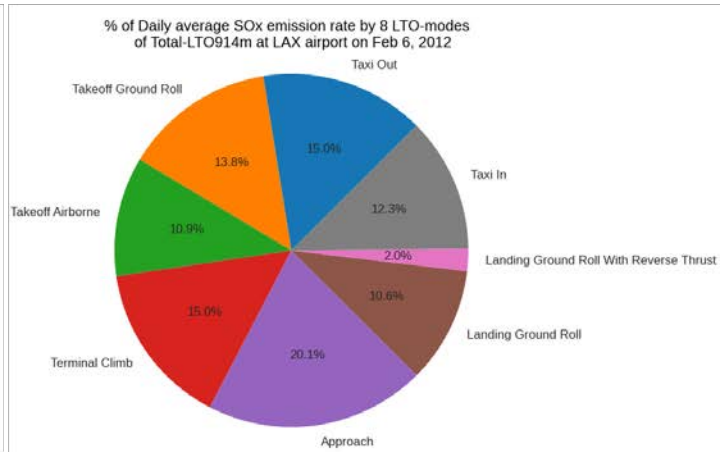
Air-layer 08		Air-source for air-layer 08 (from 700m to 800m)
...
	Air-layer 09	Air-source for air-layer 09
160	ER01R06L_TA9	Air emission (g/s) for Take-Off (T) West-to-East (06L) direction in air layer 9 (altitudes from 800 to 914.4m)
161	ER01R24R_TA9	Air emission (g/s) for Take-Off (T) East-to-West (24R) direction in air layer 9 (altitudes from 800 to 914.4m)
162	ER01R06L_LA9	Air emission (g/s) for Landing (L) West-to-East (06L) direction in air layer 9 (altitudes from 800 to 914.4m)
163	ER01R24R_LA9	Air emission (g/s) for Landing (L) East-to-West (24R) direction in air layer 9 (altitudes from 800 to 914.4m)
164	ER03R06R_TA9	Air emission (g/s) for Take-Off (T) West-to-East (06R) direction in air layer 9 (altitudes from 800 to 914.4m)
165	ER03R24L_TA9	Air emission (g/s) for Take-Off (T) East-to-West (24L) direction in air layer 9 (altitudes from 800 to 914.4m)
166	ER03R06R_LA9	Air emission (g/s) for Landing (L) West-to-East (06R) direction in air layer 9 (altitudes from 800 to 914.4m)
167	ER03R24L_LA9	Air emission (g/s) for Landing (L) East-to-West (24L) direction in air layer 9 (altitudes from 800 to 914.4m)
168	ER13R07L_TA9	Air emission (g/s) for Take-Off (T) West-to-East (07L) direction in air layer 9 (altitudes from 800 to 914.4m)
169	ER13R25R_TA9	Air emission (g/s) for Take-Off (T) East-to-West (25R) direction in air layer 9 (altitudes from 800 to 914.4m)
170	ER13R07L_LA9	Air emission (g/s) for Landing (L) West-to-East (07L) direction in air layer 9 (altitudes from 800 to 914.4m)
171	ER13R25R_LA9	Air emission (g/s) for Landing (L) East-to-West (25R) direction in air layer 9 (altitudes from 800 to 914.4m)
172	ER17R07R_TA9	Air emission (g/s) for Take-Off (T) West-to-East (07R) direction in air layer 9 (altitudes from 800 to 914.4m)
173	ER17R25L_TA9	Air emission (g/s) for Take-Off (T) East-to-West (25L) direction in air layer 9 (altitudes from 800 to 914.4m)
174	ER17R07R_LA9	Air emission (g/s) for Landing (L) West-to-East (07R) direction in air layer 9 (altitudes from 800 to 914.4m)
175	ER17R25L_LA9	Air emission (g/s) for Landing (L) East-to-West (25L) direction in air layer 9 (altitudes from 800 to 914.4m)



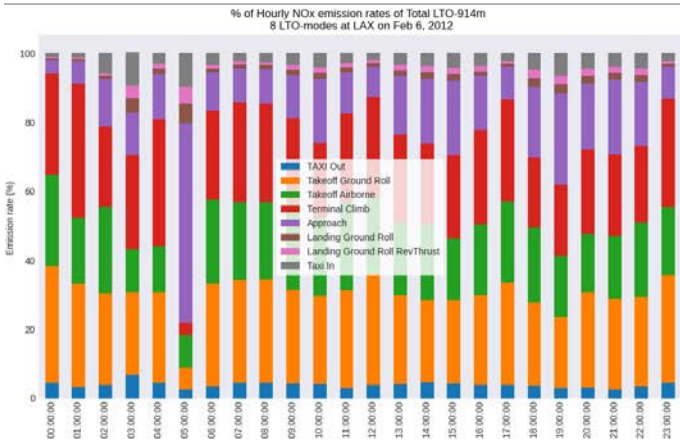
a) NOx : Daily %



b) SOx : Daily %



c) NOx : Hourly %



d) SOx : Hourly %

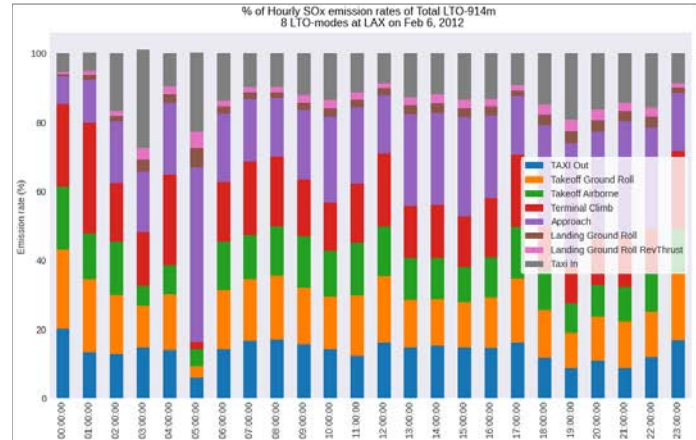
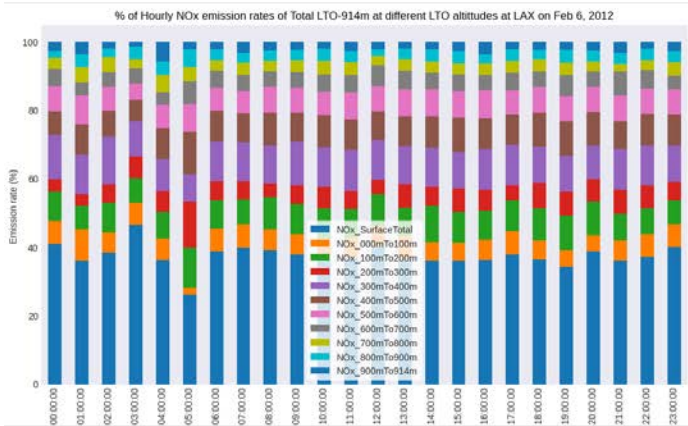
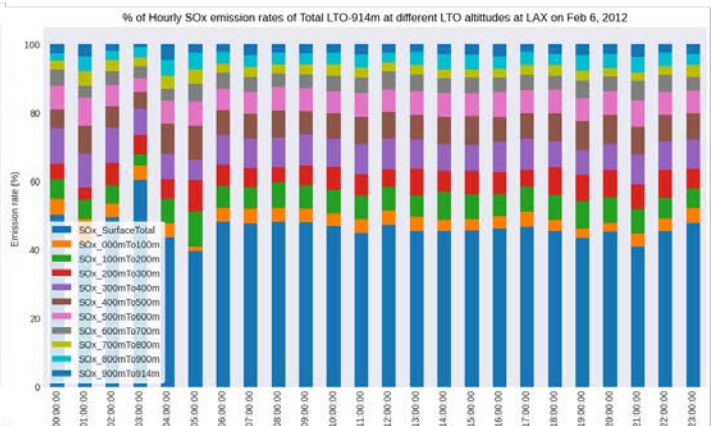


Figure A1. The % of hourly a) NOx and b) SOx of total-LTO-914m emission, the % of hourly c) NOx and d) SOx of total-LTO-914m emission in eight AEDT-LTO modes on February 6, 2012 at LAX in AEDT emission data.

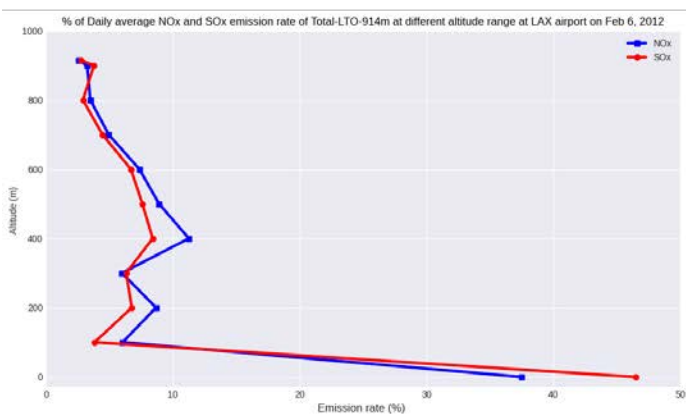
a) Hourly NOx % at different altitude



b) Hourly SOx % at different altitude



c) Daily NOx and SOx % at different altitude



d) Cumulative Daily NOx and SOx % at different altitude

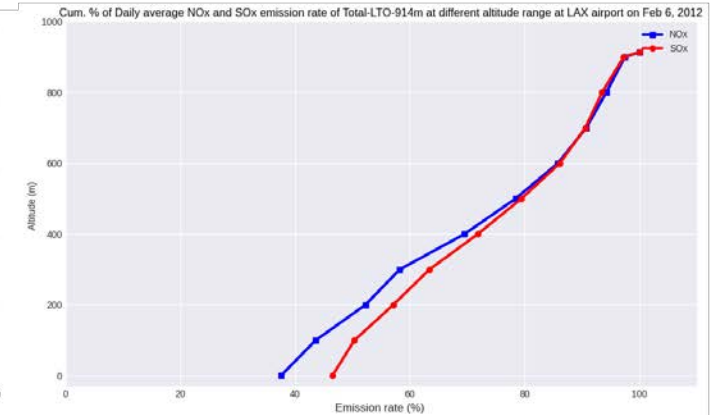


Figure A2. The % of hourly a) NOx and b) SOx of total-LTO-914m emission in different altitudes and % of daily emission of c) NOx and d) SOx of total-LTO-914m emission in different altitudes on February 6, 2012 at LAX in AEDT emission data.

Table A2. Daily total number of flights by AEDT-S and LAWA-actual (LAWA, 2020) and % change from LAWA-actual for flights at LAX on February 6, 2012.

	AEDT-S	LAWA-actual	% Change from LAWA-actual
Runway 24R/06L	359	340	5.59
Runway 24L/06R	333	295	16.84
Runway 25R/07L	450	455	-1.1
Runway 25L/07R	401	408	-1.72
LAX-total	1543	1488	3.7

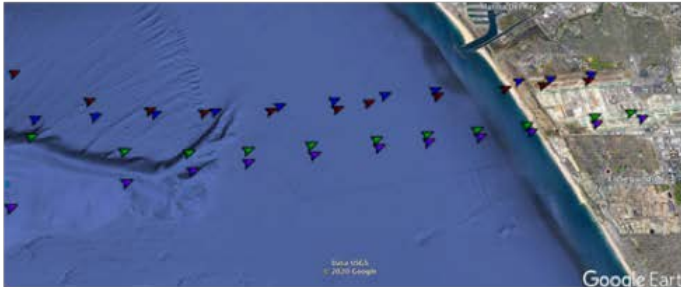


Average lat-lons in air at 9 altitudes (also 2 surface runway points given)

a) Landing: 24R (Blue), 24L (Red), 25R (Green), 25L (Purple) b) Take-Off: 24R (Blue), 24L (Red), 25R (Green), 25L (Purple)



c) Landing: 06L (Blue), 06R (Red), 07L (Green), 07R (Purple) d) Take-Off: 06L (Blue), 06R (Red), 07L (Green), 07R (Purple)



Sources in air: 9 Altitudes : 100m, 200m, 300m, 400m, 500m, 600m, 700m, 800m, 914m
 Source at surface: 1st 2-points (for take-off) and last 2 points (for landing) at the runway

Figure A3. Latitude–longitude (lat-lons) pairs of each of the nine, air layer height for eight runways and two LTOs (produced based on aircraft location data for February 2012. (These latitude–longitude pairs are assumed to be fixed for all 29 days of February to be used in the model at any hour.)